GLOBAL START-TO-END OPTIMIZATION WITH BAYESIAN OPTIMIZATION*

B. Veglia†, B. Beutner, S. Tomin, S. D. Walker,
Deutsches Elektronen-Synchrotron DESY, Hamburg, Germany

Abstract

Controlling the beam longitudinal phase space (LPS) distribution is crucial for advanced free-electron laser operation modes. At the European XFEL, this task is particularly challenging due to the complex compression scheme, which includes three bunch compressors. We present an approach based on Bayesian optimisation that streamlines the search for compression configurations yielding current profiles with desirable features, such as a flat top or a pronounced spike at either the head or the tail of the bunch. Moreover, this method can also be applied to tune the RF parameters in start-to-end simulations to achieve better agreement with measured longitudinal phase space profiles.

INTRODUCTION

Precise control over the longitudinal phase space (LPS) distribution of electron bunches is fundamental to the operation of modern X-ray free-electron lasers (FELs). At facilities such as the European XFEL (EuXFEL), advanced operating modes—including the generation of attosecond pulses or specific spectral bandwidths—rely on the ability to tailor the bunch current profile with high fidelity. However, achieving this level of control is a significant challenge due to the complex multi-stage compression schemes employed, where nonlinear beam dynamics and collective effects, such as space charge and coherent synchrotron radiation (CSR), play a dominant role.

Consequently, there is a critical need for optimization algorithms that can navigate high-dimensional parameter spaces efficiently, minimizing the number of expensive "black-box" evaluations required to reach an optimal solution. Recent advances in machine learning and global optimization offer a path forward. Bayesian optimization (BO) [1,2] has emerged as a particularly effective tool for accelerator physics [3,4], characterized by its sample efficiency and ability to handle noisy or uncertain objective functions. By utilizing a surrogate model—typically a Gaussian Process—to map the parameter space, BO can identify promising regions for evaluation without the need for exhaustive grid searches. This approach is equally applicable to online tuning and offline simulation-based optimization, where the goal is to balance the trade-offs between multiple competing beam parameters.

In this work, we demonstrate the application of Bayesian optimization to the EuXFEL compression system, focusing first on the task of model calibration. We show that by automating the tuning of RF parameters within start-to-end simulations, the BO framework can efficiently reconcile physics models with experimental measurements, ensuring that simulation-based predictions accurately reflect observed machine performance. Building on this validated model, we then demonstrate how the algorithm simplifies the search for compression configurations that yield current profiles with specific, user-defined features. This includes the generation of distributions such as flat-top profiles or pronounced current spikes at the head or tail of the bunch, which are essential for advanced FEL operations.

* Work supported by the EuXFEL R&D program.
† bianca.veglia@desy.de

MODEL CALIBRATION

A set of measurements was performed at the EuXFEL where the beam compression was varied by scanning the Linac L1 chirp from -12.4 to $-4.4\,\mathrm{m}^{-1}$ in 9 steps. The chirp is defined as $\frac{-kV\sin\varphi}{E_0+V\cos\varphi}$, where φ and V are the voltage and phase of Linac L1, $E_0 = 130$ MeV is the initial energy of the beam before L1, and $k = 2\pi f/c, f = 1.3\,\mathrm{GHz}$. Details about the European XFEL three stage compression system and beam dynamics can be found in [5,6]. The non-invasive CRISP THz spectrometer [7] was used to measure the current profile at each step, obtained from the acquired spectrum through a reconstruction algorithm [8].

Table 1: Optimization Parameters and Their Bounds

Voltage of the first harmonic cavity (inj.)	±	2.5 MeV
Phase of the first harmonic cavity (inj.)	±	0.3 deg
Voltage of the high harmonic cavity (inj.)	±	2 MeV
Phase of the high harmonic cavity (inj.)	±	0.3 deg
Voltage in L1	±	5 MeV
Phase in L1	±	0.3 deg
Voltage in L2	±	15 MeV
Phase in L2	±	0.5 deg

We implemented a BO framework to tune OCELOT simulations [9–11] by identifying the optimal parameters required to reproduce the observed beam characteristics. The optimization parameters included the RF settings for the injector and linacs L1 and L2. The optimizer was implemented using the `scikit-optimize` Python package, utilizing Message Passing Interface (MPI) parallelization on the DESY high-performance computing cluster to accelerate the process by simultaneously evaluating hundreds of simulations.

In each subprocess, the optimizer executes an OCELOT particle tracking simulation and returns a scalar score for minimization. The objective function is defined as the Root Mean Square Error (RMSE) between the reference and simulated current profiles. To ensure a robust comparison, a cross-correlation function aligns the two curves by identifying the temporal shift that maximizes their overlap.

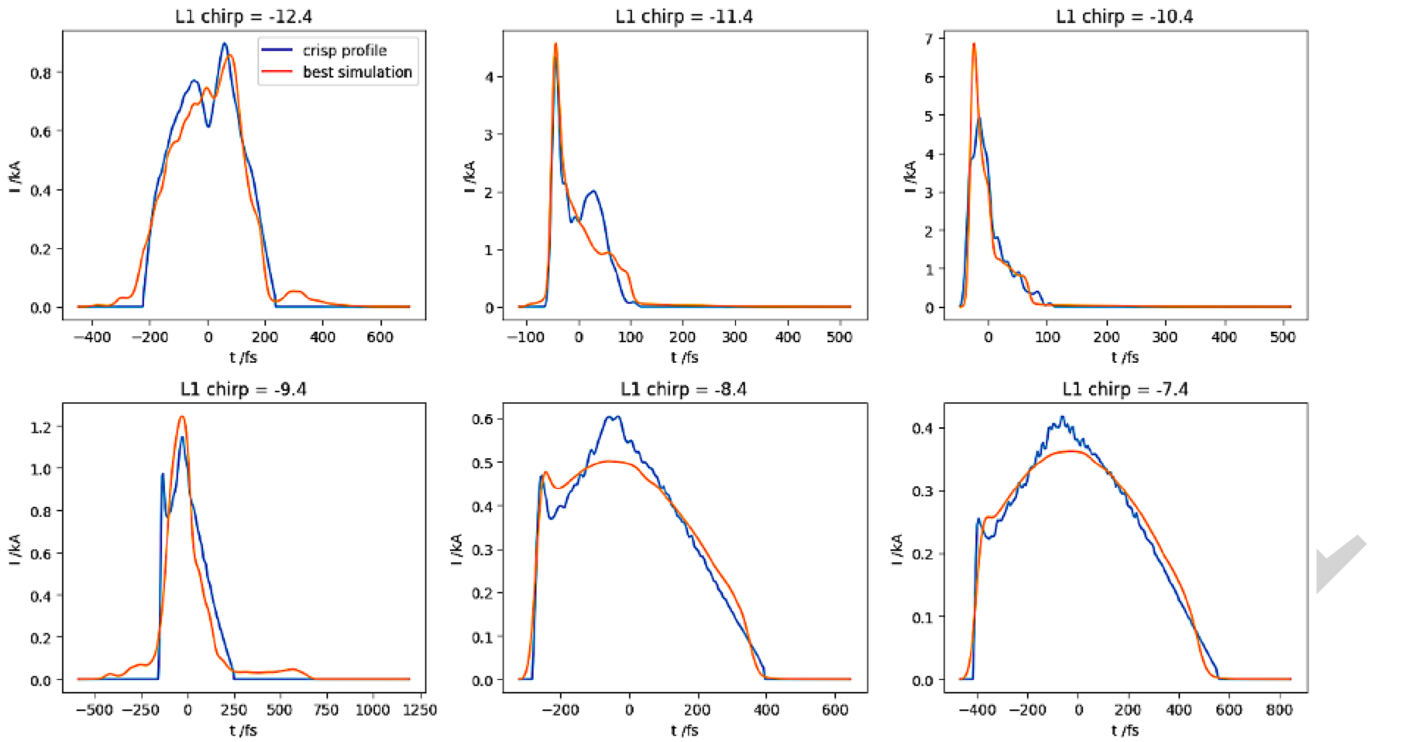

Figure 1: Comparison of optimized simulations vs current profiles measured with the CRISP spectrometer. Each plot corresponds to a different value of the chirp in L1.

Table 1 details the optimized RF parameters and their tuning ranges, defined relative to the initial machine read-outs at the time of the experiment: at the injector the $\text{chirp}_{INJ} = -8.938$, the curvature = 280 and the skewness = 21000, at linac L1 the $\text{chirp}_{L1} = -9.62$ and at the linac L2 $\text{chirp}_{L2} = -11.43$. These ranges are intentionally narrow to account for plausible instrumentation offsets or calibration errors. As shown in Fig. 1, the optimizer successfully identified the RF configurations necessary to reproduce the measured current profiles. While three of the subplots corresponding to chirps ([-6.4, -5.4, -4.4]) were omitted for brevity, they showed similar agreement (and closely resemble the curves shown in the plot corresponding to L1 chirp = -7.4). Minor discrepancies can be attributed to the fact that measurements were taken with the laser heater deactivated. The resulting microbunching instabilities are not currently modeled in the OCELOT tracking simulations, leading to small differences in the fine structure of the current profiles.

USER DEFINED PROFILES

Beyond standard parameter optimization, this same BO framework can be used to calibrate simulations against user-defined target profiles. It allows to 'reverse-engineer' simulation settings by inputting a desired output profile and letting the algorithm identify the necessary input configurations. This feature can be particularly valuable for experiments like hard X-ray self-seeding (HXRSS) [12] which are highly sensitive to the electron beam's longitudinal distribution [13].

Figure 2 shows the performance of the BO when optimizing for different reference profiles. We observed that the convergence of the optimizer is highly sensitive to the initial parameters and the choice of hyperparameters. To achieve reliable results, it was necessary to employ the "Probability of Improvement" (PI) acquisition function with high values for ξ and κ parameters (set to 10^4), which encourages a more thorough exploration of the parameter space.

CONCLUSION

In this study, we demonstrated the versatility of Bayesian Optimization as a tool for both model calibration and beam shaping at the European XFEL. The BO framework successfully reconciled start-to-end OCELOT simulations with experimental CRISP measurements by identifying small but significant offsets in RF parameters. Furthermore, the framework proved capable of "reverse-engineering" machine configurations to match specific, user-defined longitudinal current profiles, including Gaussian, flat-top, and triangular distributions.

Looking forward, we intend to utilize this BO-based methodology for systematic benchmarking of the EuXFEL simulation models across a wider range of operating conditions. By analyzing the parameter shifts required to match experimental data, the framework serves as a diagnostic tool for identifying machine imperfections, such as calibration errors or phase/voltage offsets in the RF systems. To further refine these benchmarks and minimize current profile discrepancies, new measurement campaigns are planned in which the microbunching instability (MBI) will be fully suppressed using the laser heater. This will facilitate a more direct comparison with numerical models and provide a

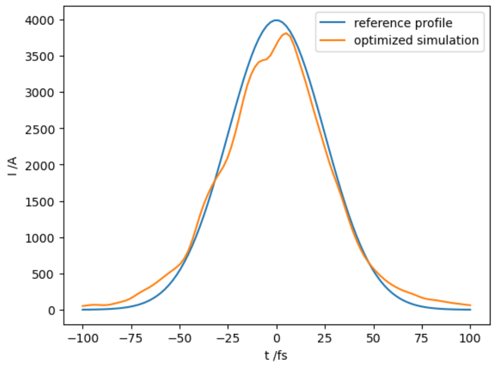

(a) Gaussian

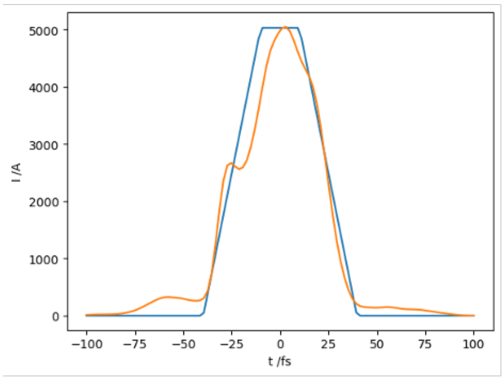

(b) Flat top

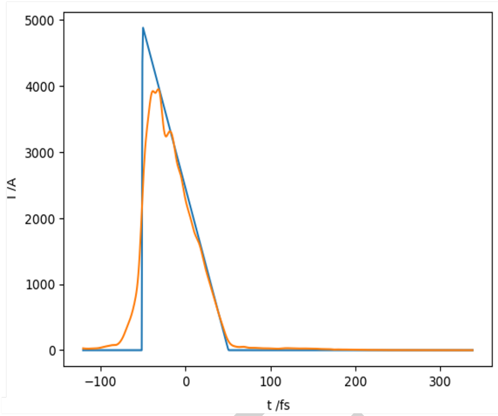

(c) Left triangle

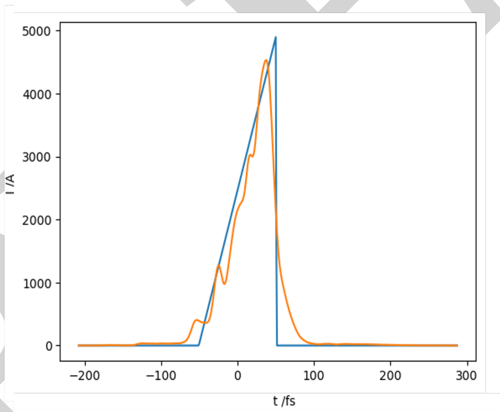

(d) Right triangle

Figure 2: Examples of simulations optimized to fit reference profiles.

clearer understanding of the underlying longitudinal dynamics.

ACKNOWLEDGEMENTS

The authors are thankful for the support through the Maxwell computational resources operated at DESY.

REFERENCES

[1] B. Shahriari, K. Swersky, Z. Wang, R. P. Adams, and N. de Freitas, "Taking the human out of the loop: a review of bayesian optimization", *Proceedings of the IEEE*, vol. 104, pp. 148–175, 2016. https://api.semanticscholar.org/CorpusID:14843594

[2] S. Greenhill, S. Rana, S. Gupta, P. Vellanki, and S. Venkatesh, "Bayesian optimization for adaptive experimental design: a review", *IEEE Access*, vol. 8, pp. 13937–13948, Jan. 2020. doi:10.1109/ACCESS.2020.2966228

[3] R. Roussel *et al.*, "Bayesian Optimization Algorithms for Accelerator Physics", *Phys. Rev. Accel. Beams*, vol. 27, no. 8, p. 084801, 2024. doi:10.1103/PhysRevAccelBeams.27.084801

[4] F. Ji *et al.*, "Multi-objective Bayesian active learning for MeV-ultrafast electron diffraction", *Nature Commun.*, vol. 15, no. 1, p. 4726, 2024. doi:10.1038/s41467-024-48923-9

[5] I. Zagorodnov and M. Dohlus, "Semianalytical modeling of multistage bunch compression with collective effects", *Phys. Rev. Spec. Top. Accel. Beams*, vol. 14, no. 1, p. 014403, Jan. 2011. doi:10.1103/PhysRevSTAB.14.014403

[6] I. Zagorodnov, M. Dohlus, and S. Tomin, "Accelerator beam dynamics at the European X-ray Free Electron Laser", *Phys. Rev. Accel. Beams*, vol. 22, no. 2, p. 024401, Feb. 2019. doi:10.1103/PhysRevAccelBeams.22.024401

[7] S. Wesch, B. Schmidt, C. Behrens, H. Delsim-Hashemi, and P. Schmüser, "A multi-channel THz and infrared spectrometer for femtosecond electron bunch diagnostics by single-shot spectroscopy of coherent radiation", *Nucl. Instrum. Methods Phys. Res., Sect. A*, vol. 665, pp. 40–47, 2011. doi:10.1016/j.nima.2011.11.037

[8] B. Schmidt, N. M. Lockmann, P. Schmüser, and S. Wesch, "Benchmarking coherent radiation spectroscopy as a tool for high-resolution bunch shape reconstruction at free-electron lasers", *Phys. Rev. Accel. Beams*, vol. 23, no. 6, p. 062801, Jun. 2020. doi:10.1103/PhysRevAccelBeams.23.062801

[9] S. Tomin, I. Agapov, M. Dohlus, and I. Zagorodnov, "OCELOT as a Framework for Beam Dynamics Simulations of X-Ray Sources", in *Proc. IPAC'17*, Copenhagen, Denmark, May 2017, pp. 2642–2645. doi:10.18429/JACoW-IPAC2017-WEPAB031

[10] I. Agapov, G. Geloni, S. Tomin, and I. Zagorodnov, "OCELOT: A software framework for synchrotron light source and FEL studies", *Nucl. Instrum. Methods Phys. Res. A*, vol. 768, pp. 151–156, 2014. doi:10.1016/j.nima.2014.07.047.

[11] I. Zagorodnov, S. Tomin, Y. Chen, and F. Brinker, “Experimental validation of collective effects modeling at injector section of X-ray free-electron laser”, *Nucl. Instrum. Methods Phys. Res., Sect. A*, vol. 995, p. 165111, 2021. doi:10.1016/j.nima.2021.165111

[12] S. Liu *et al.*, “Updates on the hard x-ray self-seeding at the european XFEL”, *Synchrotron Radiat. News*, vol. 38, no. 2, pp. 11–16, 2025. doi:10.1080/08940886.2025.2472607

[13] T. Long *et al.*, “Control of bandwidth and signal-to-noise ratio for hard-X-ray self-seeded free-electron lasers”, *Phys. Rev. Appl.*, vol. 23, no. 4, p. 044038, Apr. 2025. doi:10.1103/PhysRevApplied.23.044038